Master's Thesis
석사 학위논문

Artificial Photosynthesis:
Photocatalytic Conversion of CO_2 into Hydrocarbon Fuels

HyeRim Kim(김 혜 림 金 惠 林)

Department of Energy Systems Engineering
에너지시스템공학전공

DGIST

2014

Master's Thesis
석사 학위논문

Artificial Photosynthesis:
Photocatalytic Conversion of CO_2 into Hydrocarbon Fuels

HyeRim Kim(김 혜 림 金 惠 林)

Department of Energy Systems Engineering
에너지시스템공학전공

DGIST

2014

Artificial Photosynthesis: Photocatalytic Conversion of CO_2 into Hydrocarbon Fuels

Advisor : Professor Su-il In

Co-advisor : Ph.D Soo-Keun Lee

by

HyeRim Kim
Department of Energy Systems Engineering
DGIST

A thesis submitted to the faculty of DGIST in partial fulfillment of the requirements for the degree of Master of Science in the Department of Energy Systems Engineering. The study was conducted in accordance with Code of Research Ethics[1]

07. 18. 2014

Approved by

Professor Su-il In (Signature)
(Advisor)

Ph.D Soo-Keun Lee (Signature)
(Co-Advisor)

[1] Declaration of Ethical Conduct in Research: I, as a graduate student of DGIST, hereby declare that I have not committed any acts that may damage the credibility of my research. These include, but are not limited to: falsification, thesis written by someone else, distortion of research findings or plagiarism. I affirm that my thesis contains honest conclusions based on my own careful research under the guidance of my thesis advisor.

Artificial Photosynthesis:

Photocatalytic Conversion of CO_2 into Hydrocarbon Fuels

HyeRim Kim

Accepted in partial fulfillment of the requirements for the degree of Master of Science.

07. 18. 2014

Head of Committee ________________(인)

Prof. Su-il In

Committee Member ________________(인)

Ph.D Soo-Keun Lee

Committee Member _______________(인)

Prof. Sangaraju Shanmugam

MS/ES
201224009

김 혜 림. HyeRim Kim. Artificial Photosynthesis: Photocatalytic Conversion of CO_2 into Hydrocarbon Fuels. Department of Energy Systems Engineering. 2014. 23 p. Advisors Prof. Su-Il In, Co-Advisors Ph.D Soo-Keun Lee.

ABSTRACT

One of the major problems concerning environmental pollution and global warming is a rapid escalation in the level of carbon dioxide in atmosphere. The atmospheric CO_2 level can be reduced by converting it into useful products via thermochemical and photochemical processes. Amongst these conversion processes, the photochemical conversion is an environment effective and preferred process for the photoreduction of CO_2 into useful liquid fuels like methanol, formaldehyde, and methane gas. Photoreduction of CO_2 into hydrocarbon fuels on the surface of photocatalyst is one of the breakthroughs in the field of photocatalysis. At present various approaches have been investigated with the aim of increasing the CO_2 conversion efficiency. The reactor for photoconversion of CO_2 plays a vital role in experimental setup. In first study an attempt was made to testify a newly designed the photoreactor for conversion of CO_2 into useful products. The photoreactor was specifically designed for simple operation bearing features of temperature and pressure control. The reactor has been tested successively with the standard titania, Degussa P25 yielding methane with moderate production rate of 1007 $\mu mol \cdot g^{-1} \cdot h^{-1}$ (16.11 $ppm \cdot g^{-1} \cdot h^{-1}$). under UVB lamp (λ_{max} = 365 nm). The methane yield obtained is comparable to the values reported in literature. In second study, CuO-TiO_2 nanostructure, a hybrid material photocatalyst was synthesized and tested for CO_2 photoreduction. The synthesis process involves the formation CuS nanostructure using electrochemical anodization followed by embedment of titanium isopropoxide as Ti precursor. The oxidation of the nanosctuctre is performed at temperature of 400 °C oxidizing Cu and Ti to form CuO-TiO_2 nanostructures.

Keywords: Photocatalyst, Carbon dioxide conversion, Artificial photosynthesis, Photoreactor, Tandem CuO-TiO_2 nanostructure.

Contents

Figures

1. INTRODUCTION

1.1 Background

One of the recent problems concerning people is the sharp escalation in the level of carbon dioxide in regards to global warming. Industrial development and economic activity is increasing fossil fuel consumption [1]. It is known that the contribution to the greenhouse effect from carbon dioxide accounts for more than 80%, currently, the concentration of carbon dioxide in the atmosphere is 400 ppm, but after 30 to 40 years it is expected to reach 550 ppm. To solve this problem, the Kyoto Protocol was negotiated in 1997 to limit or reduce the emissions of four greenhouse gases (GHG) (carbon dioxide, methane, nitrous oxide, sulphur hexafluoride) and two groups of gases (hydrofluorocarbons and perfluorocarbons) [2]. Various approaches have been investigated for reducing the concentration of atmospheric CO_2 to an adequate level by following two key research streams [3-4]: (1) CO_2 capturing and (2) its transformation into useful products.

1.2 Photocatalytic CO_2 Conversion

The later research stream employs two main processes; thermochemical and photochemical for conversion of CO_2 into useable products. The thermochemical process is less preferred for the reasons of being energetically intensive and costly. The photochemical conversion is a cost effective and preferred process for the photoreduction of CO_2 into useful liquid fuels like methanol, formaldehyde, and methane gas.

In 1979, it was reported that carbon dioxide (CO_2) could be photochemically converted into several organic compounds using various materials such as TiO_2, ZnO, CdS, SiC, and WO_3 as photocatalyst [5]. In the wake of this paper, many researchers have studied how to develop an artificial photocatalyst that can convert carbon dioxide into hydrocarbon fuel using solar energy [6-7].

The possible photocatalytic reactions involved in photoreduction of CO_2 into CH_4 can be explained on the basis of the commonly accepted two electron scheme [8]. Upon illumination, photocatalyst absorbs light and generates pairs of photoexicted electrons (e^-) and holes (h^+) which can be trapped by appropriate photocatalyst sites (Equation (1)). Meanwhile, the holes react with water giving rise to oxygen and protons (Equation (2)). CO_2 molecules can then interact with the electrons and protons to give methane or other useful products (Equation (3)).

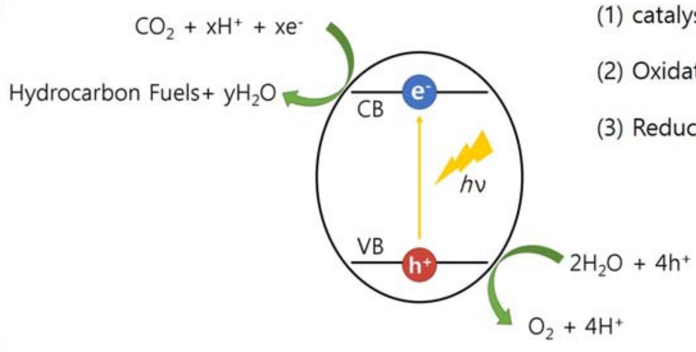

(1) catalyst + $h\nu \rightarrow$ catalyst* ($e^- + h^+$)

(2) Oxidation $H_2O + 2h^+ \rightarrow 1/2O_2 + 2H^+$

(3) Reduction $CO_2 + 2H^+ + 2e^- \rightarrow HCOOH$

$CO_2 + 2H^+ + 2e^- \rightarrow CO + H_2O$

$CO_2 + 4H^+ + 4e^- \rightarrow HCHO + H_2O$

$CO_2 + 6H^+ + 6e^- \rightarrow CH_3OH + H_2O$

$CO_2 + 8H^+ + 8e^- \rightarrow CH_4 + 2H_2O$

To convert the carbon dioxide into hydrocarbon, the bandgap of a photocatalyst must straddle the redox potentials of each half reaction [2, 6].

1.3 Electrochemical Anodization

Electrochemical anodization is a simple, low cost and high-throughput method currently used to generate arrays of vertically oriented, self-organized nanopores and nanotubes in a variety of metal oxides. This includes, but is not limited to, Al_2O_3, TiO_2, Nb_2O_5, Ta_2O_5, Fe_2O_3, WO_3, ZrO_2 and HfO_2.29. Key advantages of anodization include the availability of multiple process variables such as the temperature, duration, electrolyte composition, anodization potential (or current), anodization ramp (or pulse) sequence and substrate patterning, to control the rates of competing processes and thereby obtain a tunable and reproducible morphology at the nanoscale. Anodization has not been hitherto employed for the growth of vertically oriented nanostructures in copper sulfide (CuS and Cu_2S).

2. RESEARCH EQUIPMENT

2.1 X-Ray Diffractometer (XRD)

X-Ray diffraction is a characterization analysis method that measures the crystallographic structure, lattice parameters, planar spacing, and crystallite size of materials. This method is based on the principle of Bragg's law, when atoms is collide with incident X-ray at different angle, intensity of X-ray is increased or decreased in specific angle.

XRD is consisted of X-ray Generator, Goniometer for measuring the angle, Detector for measuring the intensity of X-ray, Control/Data Processing Unit and Computer. X-ray produce that accelerated electron by means of high voltage is crushed to metal target in the vacuum state. At that time most kinetic energy of electron is transferred to heat, 0.1% of electron is transferred to X-ray for using analysis.

XRD was measured on all the sample using a MiniFlex600 X-ray diffraction system that utilized Cu Kα radiation with λ= 1.54 Å. Samples were in film form, and scans were run from 2Θ values of 10º to 90º at a rate of 2º per minute.

Figure 1. Rigaku Miniflex 600 X-Ray Diffractometer

2.2 X-ray Photoelectron Spectrometer (XPS)

X-ray photoelectron spectroscopy is an analytical method that measures the valence states, elemental composition and the empirical formula of the elements that are present within a material. XPS spectra are measured by crushing a material with X-rays while simultaneously measuring the kinetic energy and the number of electrons that escape from the material.

XPS spectrum consists of the number of electrons detected versus the binding energy of the electrons detected. Each element produces a characteristic set of XPS peaks at characteristic binding energy values that directly identify each element that exists in or on the surface of the material being analyzed. These characteristic spectral peaks correspond to the electron configuration of the electrons within the atoms, e.g., 1s, 2s, 2p, 3s, etc. The number of detected electrons in each of the characteristic peaks is directly related to the amount of element within the XPS sampling volume.

Figure 2. Thermo ESCALAB 250Xi

XPS experiments were performed on ESCALAB 250Xi. With monochromatic incident x-rays and detectors limit of energy resolution < 0.3 eV, improper calibration or shifts due to surface charging can cause incorrect identification of surface phases. At that time XPS spectrum is compensated for using C 1s region.

2.3 Scanning Electron Microscope (SEM)

Scanning electron microscope is a type of electron microscope that obtains images of a sample by collecting the secondary electron when a focused beam of electrons is injected to sample. SEM can achieve resolution better than 1 nanometer. SEM is consisted of electron gun for making and accelerating electron, electromagnetic lens for magnification, signal detector, high-voltage generator for supplying the voltage to electron gun and filament, stage, holder and vacuum system.

The samples were measured by using Hitachi S-4800 High Resolution Scanning Electron Microscope. The S-4800 is a cold field emission high resolution scanning electron microscope that can guarantee high resolution (1.4 nm) at low voltage. The accelerating voltage on the S-4800 is around 0.5 - 30 kV. The S-4800 has a specimen stage X = 0 ~ 50mm and Y = 0 ~ 50mm. The SEM utilizes vacuum conditions and uses electrons to form a high image resolution, special preparations was done to the samples. All samples, before and after the reaction, were totally dried from moisture to avoid the vaporization in the vacuum. Moreover, all samples were coated with a thin layer of conductive material (Platinum). This coating process was done by using a device called a sputter coater (HITACHI MC1000, coating condition: 15 μ A 30 sec).

Figure 3. Hitachi S-4800 High Resolution Scanning Electron Microscope

2.4 Transmission Electron Microscope (TEM)

Transmission Electron Microscopy is a microscopy technique in which a beam of electrons is transmitted through an ultra-thin specimen, interacting with the specimen as it passes through. TEM functions by generating a primary electron beam of high energy and high intensity that passes through a condenser to produce parallel beams that irradiate the sample. Magnified images of the sample are formed by combining the transmitted electrons using an electromagnetic objective lens. TEM is primarily used to give information on topography, morphology and crystal structure at with atomic resolution (0.1 nm).

The TEM micrographs were recorded on a Hitachi HF 3300 High Resolution Transmission Electron Microscope operating at 100 kV using formvar/carbon coated nickel grids. For making the thin sample in the chapter 4, the CuO-TiO_2 foil is sonicated in the ethanol and the solution including CuO-TiO_2 structure is dropped in the nickel grid and dry at room temperature for 30 min.

Figure 4. Hitachi HF 3300 High Resolution Transmission Electron Microscope

3. Photocatalytic conversion of CO_2 into hydrocarbon fuels with standard titania (Degussa P25) using newly installed experimental setup

3.1 Introduction

Energy is the “fuel of life.” It exists all around us in various forms such as heat, light and electricity. Living organisms must acquire energy in the form of minerals, proteins, carbohydrates etc. to survive on this earth. Most of the energy is generated from non-renewable resources like coal, fossil fuel oils, natural gas and nuclear resources (radioactive elements). Currently a large portion of energy in terms of heat and electricity arrives from oil and gas reserves. One of the key pollutants generated by the consumption of fossil fuels is CO_2 [9]. Utilization of fossil fuels and various industrial processes emit CO_2 leading to a rise in the level of atmospheric CO_2. Such emissions causes the serious issues of global warming and environmental pollution [2, 9].

Various approaches have been investigated for reducing the concentration of atmospheric CO_2 to a normal level by following two key research streams [3, 10]: (1) CO_2 capturing and (2) its transformation into useful products. The later research stream employs two main processes, thermochemical and photochemical for conversion of CO_2 into useable products. The thermochemical process is less preferred for the reasons of energetically intensive and costly. While, the photochemical conversion is an environment effective and preferred process for the photoreduction of CO_2 into useful liquid fuels like methanol, formaldehyde, and methane gas [4-5, 11-12]. Unfortunately, the yield of photochemical conversion product is much less. Thus requires gigantic efforts for improving the CO_2 photoreduction efficiency. Therefore, the photochemical reduction of CO_2 has the dual advantage of reducing atmospheric CO_2 concentration and producing useful products. However, the conversion efficiency still very low. An extensive amounts of research are being carried out to enhance the performance and productivity in this research area [10-12].

3.2 Method

The photoreduction of CO_2 was carried out using standard titania photocatalyst, Degussa P25. The experiment was performed using a newly designed photoreactor. The reactor assembly composes of a stainless steel platform, a circular photoreactor (Volume of the photoreactor = 15.4 cm^3) bearing an inlet and outlet valves. The photoreactor has two side openings covered with rubber septum for sampling purposes and a thermocouple to measure inside temperature of the photoreactor. The schematic diagram of the experimental setup is shown in Figure 5.

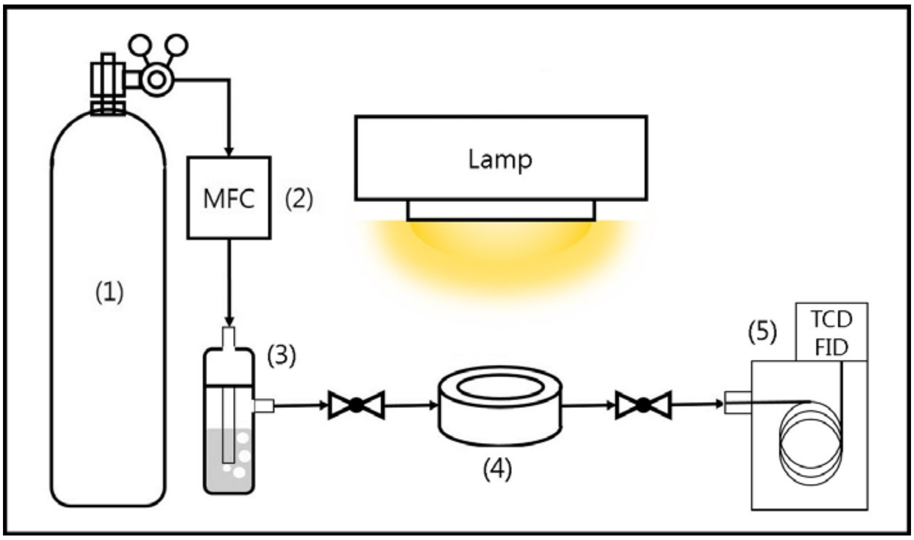

Figure 5. The schematic representation of the experimental setup for CO_2 photoreduction comprising of (1) CO_2 gas Cylinder, (2) Mass Flow Controller, (3) Gas bubbler containing deionized water, (4) Photoreactor for conversion of CO_2, (5) Gas Chromatography unit

The design of the photoreactor assembly is shown in Figure 6. The experimental setup consists of the following components:

1. CO_2 gas cylinder providing 99.999% CO_2.

2. Mass flow controller (MFC) installed in the inlet line before the reactor and a vacuum pump at the last preceding the outlet line.

3. Gas bubbler containing deionized water providing a mixture of CO_2 and H_2O to the photoreactor.

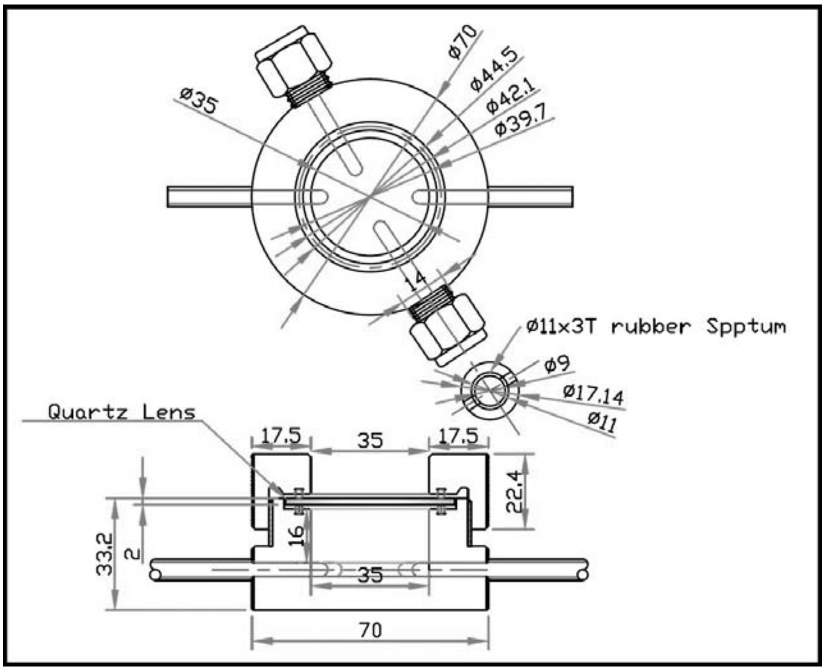

Figure 6. Design of photoreactor used for CO_2 photoconversion.

The complete experimental procedure from start to the final product involved various steps. The experimental procedure begins with the purging of the photoreactor using a vacuum pump. Both the photoreactor lines and the photoreactor are needed to be evacuated in order to remove any reactive gases or air in the reactor setup. Before the purging of the photoreactor, the line from CO_2 cylinder to the photoreactor was flushed with CO_2 for a long time to remove any air in the line if present. The CO_2 gas flow rate was controlled by a mass flow controller (MFC) installed in the feed line prior to the photoreactor as shown in Figure 5. The CO_2 was passed through the MFC and a gas bubbler containing deionized water to generate a mixture of CO_2 and H_2O. The inlet valve of the photoreactor was then closed to saturate the inlet line with CO_2 and H_2O.The flow range of the MFC was adjusted at 0-10 $mL \cdot min^{-1}$. Just after opening the valve of CO_2 cylinder, the MFC displayed a flow rate of 10 $mL \cdot min^{-1}$. As the CO_2 gas continues to flow, the flow rate was decrease and eventually reached to 0 $mL \cdot min^{-1}$. This value was achieved for the reason of achieving zero pressure difference within the system (the photoreactor and the lines). At this point it was considered that the photoreactor and inlet line was saturated with a mixture of CO_2 and H_2O. Meanwhile, the photoreactor was purged by opening the outlet valve and purging was continued till the vacuum reaches a value of 2.0×10^{-2} Torr. Upon reaching the desired vacuum value the outlet valve of the photoreactor was closed gently while the inlet valve was opened to pass CO_2 gas into it. Before the photocatalyst loading, the reactor was purged with CO_2 gas for 5 times in order to remove any air or other impurities present in the system using this method. The GC analysis of mixture gas (CO_2 and H_2O) in the photoreactor was conducted as a background test. The test shows no carbon containing compounds in the GC analysis and therefore used as reference data in further calculations.

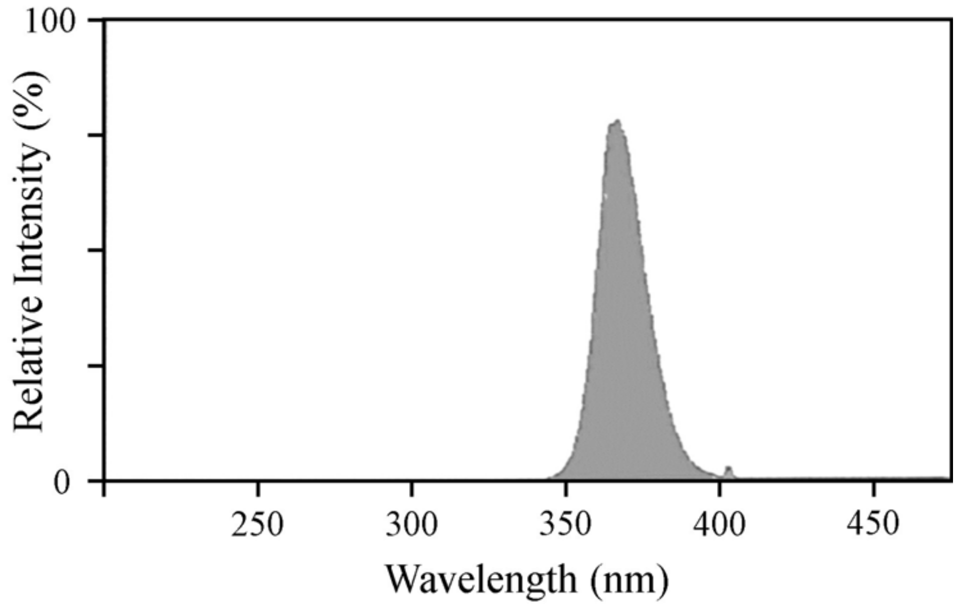

Figure 7. Spectral chart of UVB lamp (($\lambda_{\text{max intensity}}$ = 365 nm, UVP Inc. UVGL-58) referred to UVP Inc.

Afterwards the photoreactor was loaded with 50 mg of Degussa P25, the standard titania photocatalyst. The purging using high purity CO_2 gas was repeated with titania, Degussa P25 loaded the photoreactor for at least five times before illumination. The CO_2 gas from the cylinder was opened and CO_2 flows to the photoreactor through a gas bubbler containing deionized water. The photoreactor is considered to be saturated with CO_2 and H_2O mixture when MFC displays 0 $mL \cdot min^{-1}$ flow rate, indicating no further flow of CO_2 gas from CO_2 cylinder into system. At this stage the inlet valve of the photoreactor was closed and was subjected to illumination for photoreduction of CO_2 into valuable products. The illumination was carried for one hours using light from a UVB lamp ($\lambda_{\text{max intensity}}$ = 365 nm, UVP Inc. UVGL-58, light intensity: 1200 μWcm^{-2}, Figure 7). The distance between photocatalysts and UVB lamp was 3 cm. The increase in the temperature of the photoreactor under illumination and relative humidity was also measured (80 %). After one hour illumination, the final temperature of the photoreactor was found to be 35 °C. This increase in temperature was considered to have negligible effect on the photocatalytic activity of P25 [13]. The products measurement was controlled using Shimadzu GC-2014 gas chromatograph (Restek Rt-QBond column, ID=0.53 mm, length=30 m) equipped with flame ionization (FID) and thermal (TCD) detectors.

3.3 Results and Discussion

The sample of the products was taken from the photoreactor by using a syringe (500 μL). The syringe was inserted in the photoreactor through side opening enclosed with a rubber septum. The sample was then injected to the GC for product analysis. The GC analysis of the product sample shows a dominant yield of methane with minor yields of other hydrocarbons such as ethane, propane, butane. The standard titania, Degussa P25 yield methane at a production rate of 1007 $\mu mol \cdot g^{-1} \cdot h^{-1}$ (16.11 $ppm \cdot g^{-1} \cdot h^{-1}$).

The possible photocatalytic reactions involved in photoreduction of CO_2 into CH_4 can be explained on the basis of commonly accepted two electron scheme [8]. Upon illumination, TiO_2 absorbs light and generate pairs of photoexicted electrons (e^-) and holes (h^+) which can be trapped by appropriate TiO_2 sites (Eq. (1)). Meanwhile, holes reacts with water giving rise to oxygen and protons (Eq. (2)). CO_2 molecules can then interact with the electrons and protons to give methane or other useful products (Eq. (3)).

$$TiO_2 + h\nu \rightarrow e^-_{CB} + h^+_{VB} \qquad (1)$$

$$2H_2O + 4h^+ \rightarrow 4H^+ + O_2 \qquad (2)$$

$$CO_2 + 8\,H^+ + 8e^- \rightarrow CH_4 + 2H_2O \qquad (3)$$

4. Development of a Tandem TiO_2 Photocatalyst Covered with CuO Nanorods Layer for High-rate Solar Photoctalytic CO_2 Conversion to Hydrocarbon Fuels

4.1 Introduction

Carbon dioxide (CO_2) is an effective greenhouse gas because it has a serious impact on the global temperature. Current fossil fuel consumption increases atmospheric carbon dioxide concentration monotonically [14]. Hence, the control of CO_2 release into the atmosphere is required to alleviate global warming [15, 16]. Photocatalysis, an ambient temperature and environmentally friendly technique, is a feasible technology condensing the atmopsheric CO_2 and thus can minimize the impact of global warming. In addition photocatalysis can utilize sunlight for conversion of CO_2 into hydrocarbon fuels suitable for the energy infrastructure based on renewable energy policies [2, 17-18].

Many TiO_2 based materials have been tested for CO_2 conversion [7, 19, 20]. However the TiO_2 exhibits poor efficiency due to wider bandgap and high charge recombination [21, 22]. Despite of wider bandgap, the conduction band of TiO_2 appears at more negative potential than the CO/CO_2 potential [23]. Under the condition of high electron degeneracy, electrons can transfer to CO_2 from TiO_2 conduction band. Thus it is an effective strategy to couple TiO_2 with another co-catalyst which is able to take photogenerated electrons from the TiO_2 conduction band and transfer them to the adsorbed CO_2. Both platinum and copper have been selected to help charge carrier transfer between TiO_2 and the reactant species [24-26]. However instead of those metals it is useful to hire oxide photocatalysts with appropriate band positions such as Copper (II) oxide (CuO) [10]. CuO is a p-type semiconductor with a direct bandgap (E_g = 1.2 - 1.5 eV) [27]. Modification of CuO by synthetic combination with TiO_2 nanoparticles can result in multifunctional p-n heterojuctions. It is well known that coupling of the two semiconductors, CuO and TiO_2, results in 1) an enhanced stability against photocorrosion, 2) a higher separation of photogenerated charge carriers, and 3) a favorable shift of band edge [28-30].

One dimensional (1D) inorganic nano-structures have attracted considerable interest due to their unique properties such as uniform size, well-defined morphology, low density, large surface area and many potential applications [31, 32]. As catalysts they can have more active sites and adsorption properties [33]. A variety of synthetic methods have been developed to produce 1D nano structures including thermal, chemical, electrochemical and template method [34, 35]. The morphologies of the nanorods prepared by template method are similar to those of the templates. However the removal of the templates by either thermal or chemical means is very inconvenient and energy-consuming. Therefore development of the template free method is very important.

In this study it is described a new tandem type nanostructured material, TiO_2 blocks decorated with vertically aligned CuO nanorods, that photocatalytically converts CO_2 into hydrocarbon fuels (methane etc.) at ambient temperature without any novel metal co-catalyst such as Pt. A simple route was designed to fabricate the tandem nanostructure comprised of electrochemical anodization followed by thermal oxidation method. The ability to combine TiO_2 blocks and CuO nanorods, which has not previously been accomplished in related hybrid nanostructures made using such simple methods, is important to widen the wavelength range of solar radiation that can be absorbed.

4.2 Method

4.2.1 Materials

Copper substrate (Cu foil, WONIL CO., LTD., 99.9%) Titanium Foil (Ti, Sigma Aldrich, 99.7%), Sodium Sulfide (Na2S, Sigma Aldrich), Titanium isopropoxide (TTIP, $Ti[OCH(CH_3)_2]_4$, Sigma Aldrich, 97%), Carbon paper (C, CNL energy, 420 μm), Acetone, Ethanol, Distilled water

4.2.2 Synthesis

The Cu substrate (Cu foil, 99.9%, WONIL CO., LTD.) was sized 2 x 3 x 0.01 cm. Before the anodization, the Cu foil was cleaned with acetone and ethanol, followed by a deionized water rinse. The anodization was performed using a two-electrode cell with Cu foil as the working electrode and carbon paper (CNL energy, 2 x 3 x 0.042 cm) as the counter electrode. Anodizations were carried out for about 1 min at a constant applied voltage of 3 V at room temperature in an aqueous solution of 0.2 M Na_2S (Sigma Aldrich). After anodization, the Cu foil was rinsed with water, and dried at 70 °C for 1 hour. The anodized Cu foil was let in and out the titanium isopropoxide as Ti precursor, and dried at room temperature for over 12 hours. To convert the $Ti(OH)_2$ to anatase TiO_2 in the dry process, the as-prepares sample was annealed at 400 °C for 3 hours in air (flow rate of air gas: 30 $mL \cdot min^{-1}$).

4.2.3 CO_2 conversion test method

After loading the sample (2X2 cm), the reaction chamber was evacuated to about 30 mTorr. Pure CO_2 (99.999%) was introduced into the chamber through a deionized water bubbler at a total flow rate of 10 $mL \cdot min^{-1}$. The CO_2 loading/evacuation process was repeated five times. The relative standard deviation of the CO_2 concentration was about 1.5%, and the relative humidity was measured to be about 80%. A 300W Xe lamp (Newport corp. No. 66984) with an AM1.5 filter was used as a light source (light intensity: 100 $mWcm^{-2}$). After the photocatalytic reaction was allowed to proceed for three hours, quantitative detection of reactants and products was performed using a Shimadzu GC-2014 gas chromatograph (Restek Rt-QBond column, ID=0.53 mm, length=30 m) equipped with flame ionization (FID) and thermal conductivity (TCD) detectors

4.2.4 Sample analysis

To confirm the purity and crystallinity of the sample were analyzed using X-ray diffraction (XRD, Rigaku MiniFlex 600, 40kV, Cu Kα-radiation). For chemical composition analysis, X-ray photoelectron spectroscopy (XPS) studies were carried out with an ESCALAB 250Xi (Thermo) system using Al Kα (150 W) radiation. The morphologies of the samples were examined Scanning Electron Microscopy using a Hitachi S-4800 at an accelerating voltage of 3 kV. Energy Dispersive X-ray Spectroscopy (EDX) using the EDX detector on a Hitachi S-4800, operated at 20 kV. High resolution transmission electron microscopy (HRTEM, Hitachi HF-3300) were carried out to confirm distinct lattice fringes of the nanorods. The TEM sample was obtained by tearing off the sample, followed by ultrasonication in ethanol solution for 3 min. Two droplets of well-dispersed ethanol solution were deposited on the carbon coated nickel grid. The TEM sample was ready to be analyzed after being dried overnight.

4.3 Results and Discussion

Our design strategy, shown in Figure 8a, uses uniform anodized CuS dendrites as reactive substrate that are transformed to vertically aligned CuO nanorods on TiO_2 blocks.

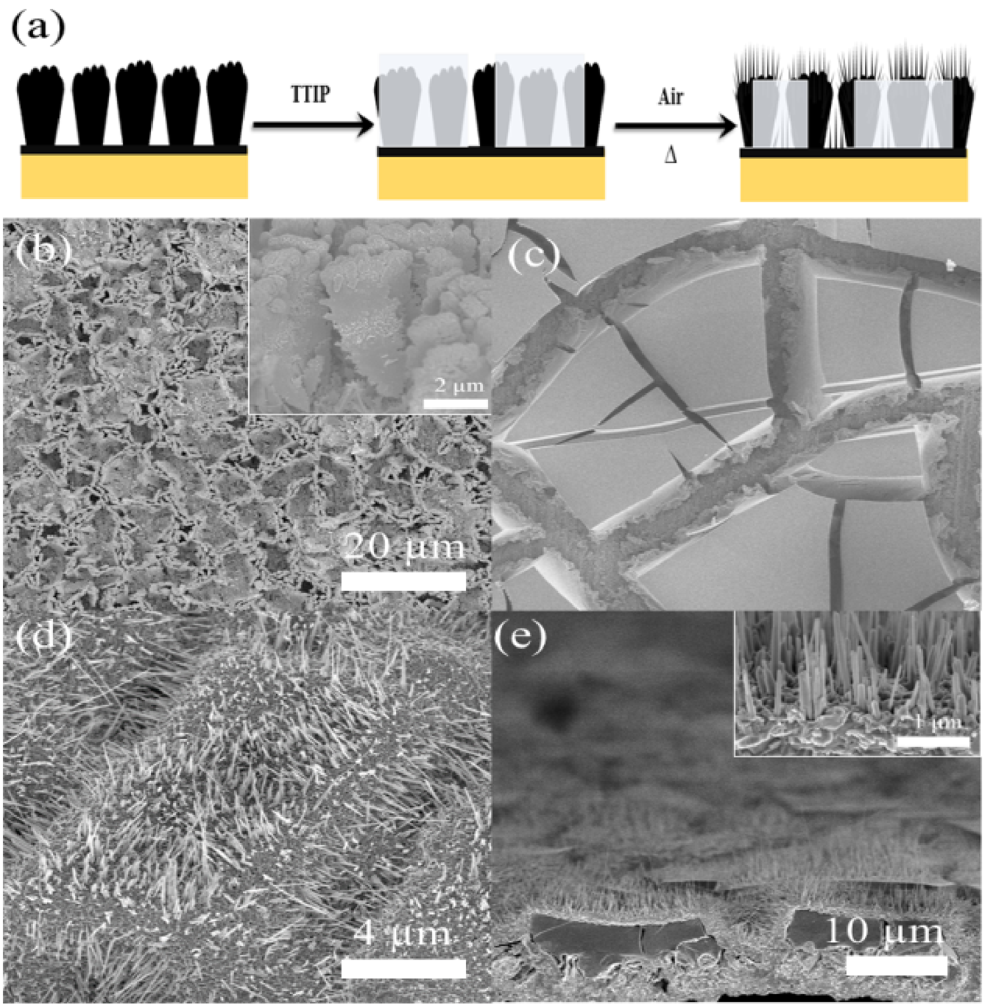

Figure 8. (a) Diagram showing the multistep strategy that convert CuS dendrites into hybrid TiO_2 blocks covered with CuO nanorods, SEM images of (b) CuS dendrites, (c) CuS dendrites covered with Ti precursor block after drying, (d) TiO_2 blocks covered with CuO nanorods, and (e) cross section of the TiO_2 blocks covered with CuO nanorods.

First CuS dendrites are synthesized by anodization of Cu foil in sulphide base aqueous electrolyte. The field emission scanning electron microscope (FESEM) images in Figure 8b shows the dendrite morphology of CuS, which can hold Ti precursor (Titanium (IV) Isopropoxide, TTIP) firmly during the thermal annealing process. Without CuS dendrites, Ti precursor is not attached on the surface of the Cu foil. Figure 8c shows top view of Ti precursor blocks on CuS dendrites. Next CuO nanorods grow on the TiO_2 block surfaces by slow annealing under air at 400 °C for 3 hours. Figure 8d shows the surface of the TiO_2 blocks-CuO nanorods. The cross-section of the TiO_2 blocks decorated with well aligned CuO nanorods is shown in Figure 8e.

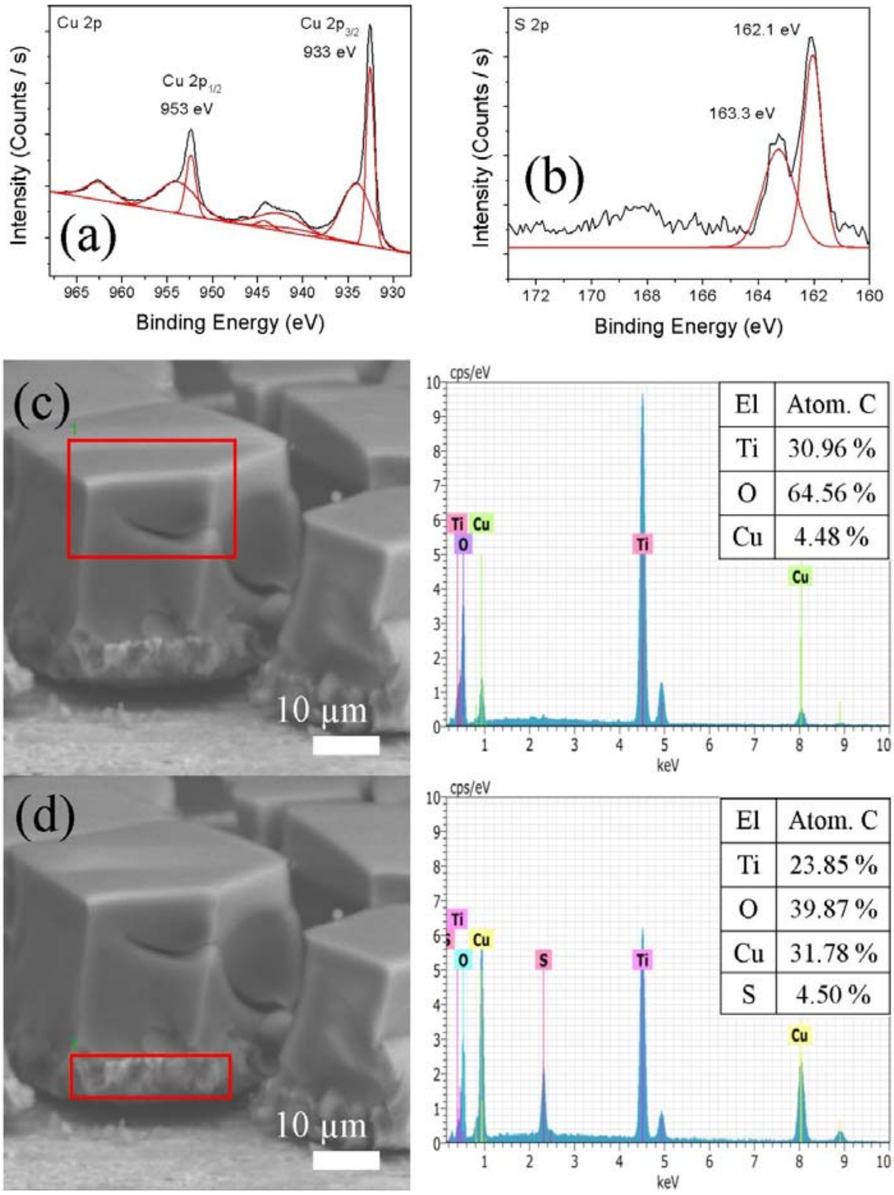

Figure 9. XPS spectra of CuS dendrite showing (a) Cu 2p and (b) S 2p regions. Cross-sectional SEM and EDS data of (c) upper side and (d) down side dried CuS dendrite covered with Ti pre-cursor blocks.

For the confirmation of presence of sulphur in the copper dendrites The XPS data of the copper dendrites was measured and is shown in Figure 9. Figure 9a shows the Cu 2p spectra with strong peaks corresponding to Cu $2p_{1/2}$ and Cu $2p_{3/2}$ at binding energies of 953 and 933 eV respectively. Figure 9b shows the S 2p spectra with two main peaks appearing at 162.1 eV and 163.3 eV. These peaks can be assigned to the Cu-S and S-S bonds respectively [36]. Thus the XPS of copper dendrites assures the presence of sulphur in the sample.

Furthermore to observe the formation of $Ti(OH)_2$ during drying, the elemental analysis was performed by electron diffraction X-ray spectroscopy (EDS) of the dried CuS dendrites covered with titanium isopropoxide as Ti precursor. The EDS data corresponding to the respective region (red squares in cross-sectional SEM images) is shown in Figure 9c and d. It can be clearly seen, the blocks of $Ti(OH)_2$ (Figure 9c) are composed mainly of Ti (30.96 %), O (64.56%) elements after drying, confirming the formation of $Ti(OH)_2$. While the elemental analysis of the copper dendrites base (figure 9d) shows the presence of sulphur which is well agreed with the XPS data.

To understand the formation of tandem nanostructure the annealing was done at various temperatures, from 100 to 400 °C. The FESEM images of the samples annealed at 100, 200, 300 and 400 °C reveals several aspects of converting TiO_2 precursor and CuS dendrites into the final product of TiO_2 blocks decorated with CuO nanorods (Figure 10). First, heating causes the TiO_2 precursor layer to crystallize and crack as shown by the samples annealed at 100 °C and 200 °C (Figure 10a and b). At 300 °C CuO nanorods grow through the cracks among the TiO_2 blocks (Figure 10c). Finally at 400 °C, the CuO nanorods moderately cover the surface of the TiO_2 blocks (Figure 10d).

The mechanism of CuO nanorods formation is not well known yet. However it is presumed here that the thermal stress promotes the outward diffusion of the Cu^{2+} ions between $Ti(OH)_2$ blocks to the $Ti(OH)_2$ surface. The Cu^{2+} ions diffusing to the surface can react with oxygen, forming CuO molecules acting as nucleation sites for CuO nanorods growth [37, 38]. At the same time, the $Ti(OH)_2$ crystallizes into TiO_2 anatase phase. CuO nanorods moderately encapsulate the TiO_2 blocks, it helps to complete p-n junction between TiO_2 (n-type semiconductor) and CuO (p-type semiconductor).

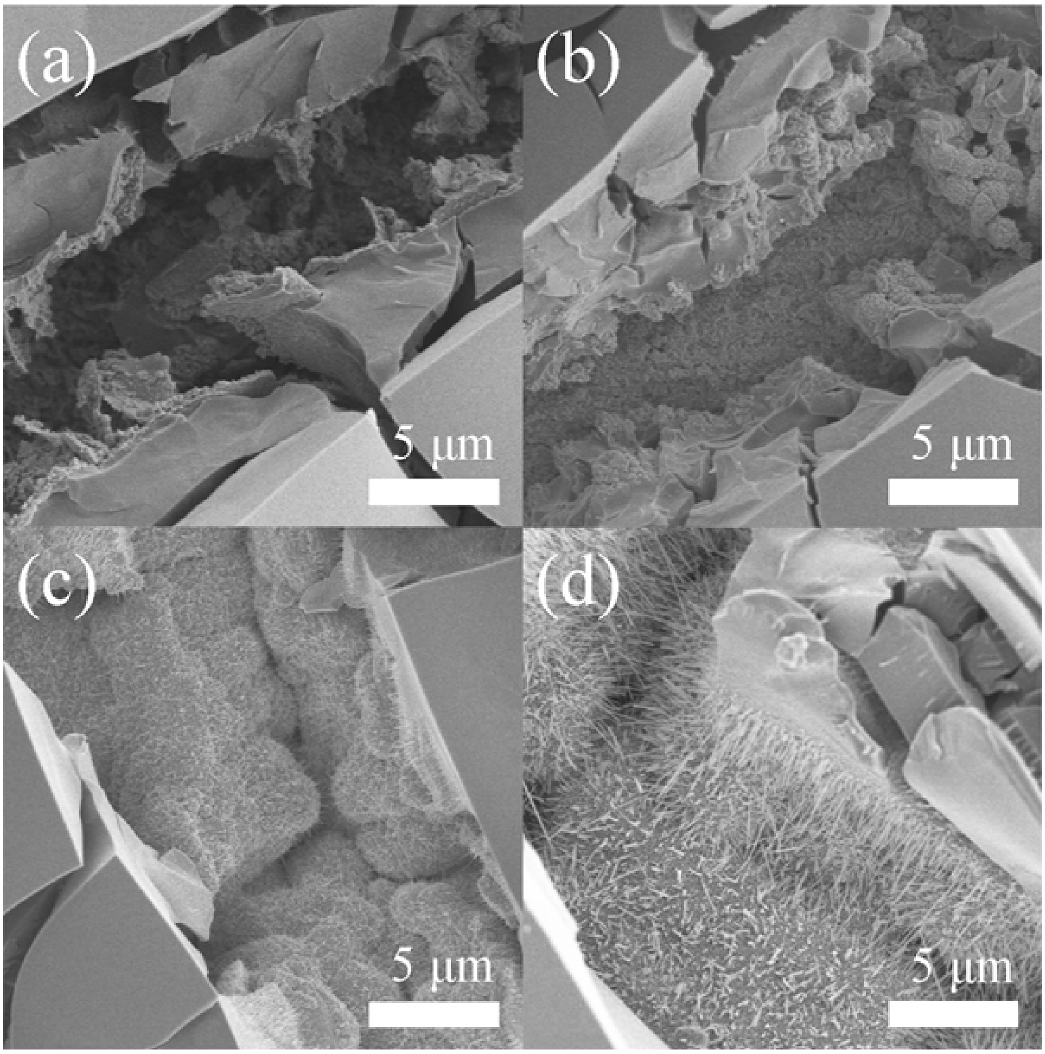

Figure 10. FESEM images of TiO_2 presursor-CuS dendrites annealed for 1 hour at (a) 100 °C, (b) 200 °C, (c) 300 °C and (d) 400 °C.

The transmission electron microscope (TEM) image in Figure 11a shows the resulting uniform (98.1 ± 20.0) nm thick nanorods. The high-resolution TEM (HRTEM) image in Figure 11b shows the middle of a representative sample. 2.32 Å lattice spacing is observed in the nanorod, which uniquely corresponds to CuO (111) [39]. Further evidence for the presence of TiO_2 and CuO comes from X-ray photoelectron spectroscopy (XPS) data. Figures 11c and d show XPS spectra for the Ti 2p and Cu 2p regions, respectively. As shown in Figure 11c, the strong peaks at around 933 eV and 953 eV are corresponding to Cu 2p3/2 and 2p1/2 peaks respectively [40]. It reveals that the chemical valences of Cu in the CuO nanoparticles are +2 valence states. Regarding TiO_2, as shown in Figure 11d, the Ti 2p region of the samples has binding energies (BEs) of 458.7 eV and 464.4 eV, attributed to the spin-orbit split (2p3/2 and 2p1/2) of the 2p core level [40, 41]. XPS data for the Ti 2p regions confirm the presence of and Ti^{4+}.

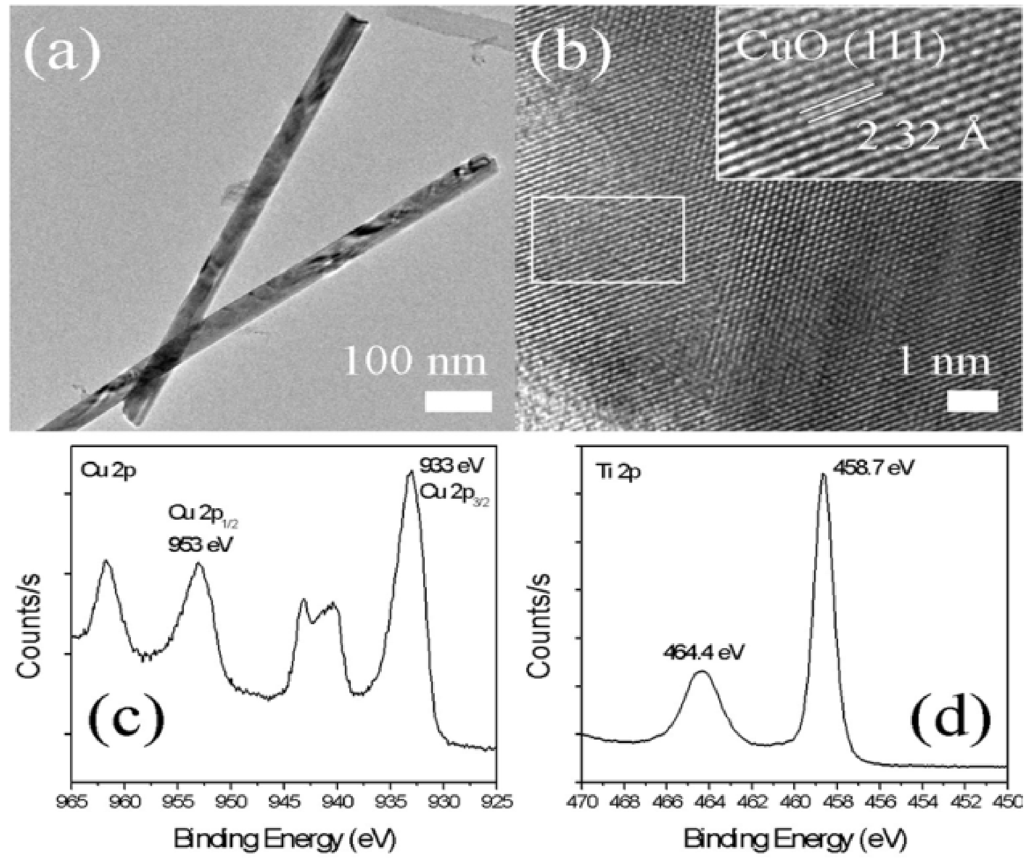

Figure 11. (a) TEM of CuO nanorods, b) HRTEM of CuO nanorods, and XPS spectra of c) Ti 2p and d) Cu 2p regions, respectively.

Control experiments show that annealing at 400 °C for 3 hours in air is optimum condition to get the final prdocut of TiO_2 blocks-CuO nanorods. X-ray diffraction (XRD) data confirms that the product is composed of Cu_2O, CuO and TiO_2 (Figure 13) [42, 43]. The inset figure shows the enlarge view of XRD in the range of 2θ = 20-45°.

However the XPS doesn't show any chemical valences of Cu due to Cu_2O which is contradicting with the XRD data (Figure 12). The XRD data shows the Cu_2O peaks along with CuO in the sample. This may be due to the depth limitation (3 μm) of XPS scan. Thus it is obvious that the surface of TiO_2 block is mainly covered by CuO nanorods while the Cu_2O exists in the core of the tandem structure. It is believed here that the photocatalytic CO_2 conversion is occurring more actively on surface rather than core. Thus the CuO nanorods on the surface of tandem structure mainly contributes for CO_2 photoconversion to hydrocarbons.

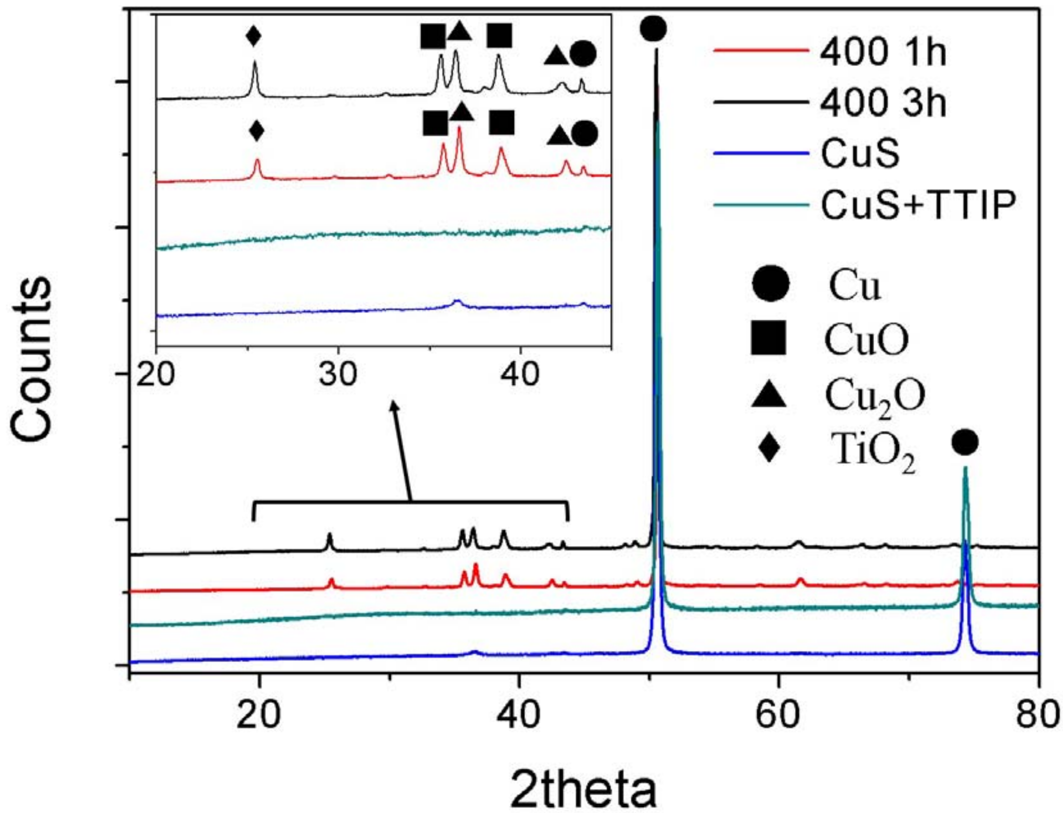

Figure 12. Powder XRD of CuS dendrite (blue), Ti precursor on the CuS dendtrite (green), TiO_2 block-CuO nanorods annealed for 3 hours (black) and 1hour (red) at 400 °C.

Photocatalytic CO_2 conversion measurements were carried out under simulated solar irradiation (AM 1.5G, 100 $mWcm^{-2}$) at ambient temperature, and reaction products were monitored by gas chromatography (GC). GC analysis of the products showed predominantly methane, along with ethane, propane, and butane as minor products.

Figure 13 shows the methane formation rates for each sample, plus additional control experiments. The optimised TiO_2 block-CuO nanorods tandem sample (e) yields 10.9 $\mu mol \cdot cm^{-2} \cdot h^{-1}$ of methane, which represents a production rate that is 5.7 times faster than that of TiO_2 synthesized that Ti foil anodized at 3V for 1min and dried at 70 °C for 1 hour and annealed at 400 °C for 1 hour (c) when measured under the same conditions (1.9 μmol·cm^{-2}·h^{-1}). The 1 hour annealed TiO_2 block-CuO tandem nanorod sample (d) yields even less methane formation rate. The CuS dendrite before annealing (a) and the annealed CuS dendrite (b) samples showed negligible activity.

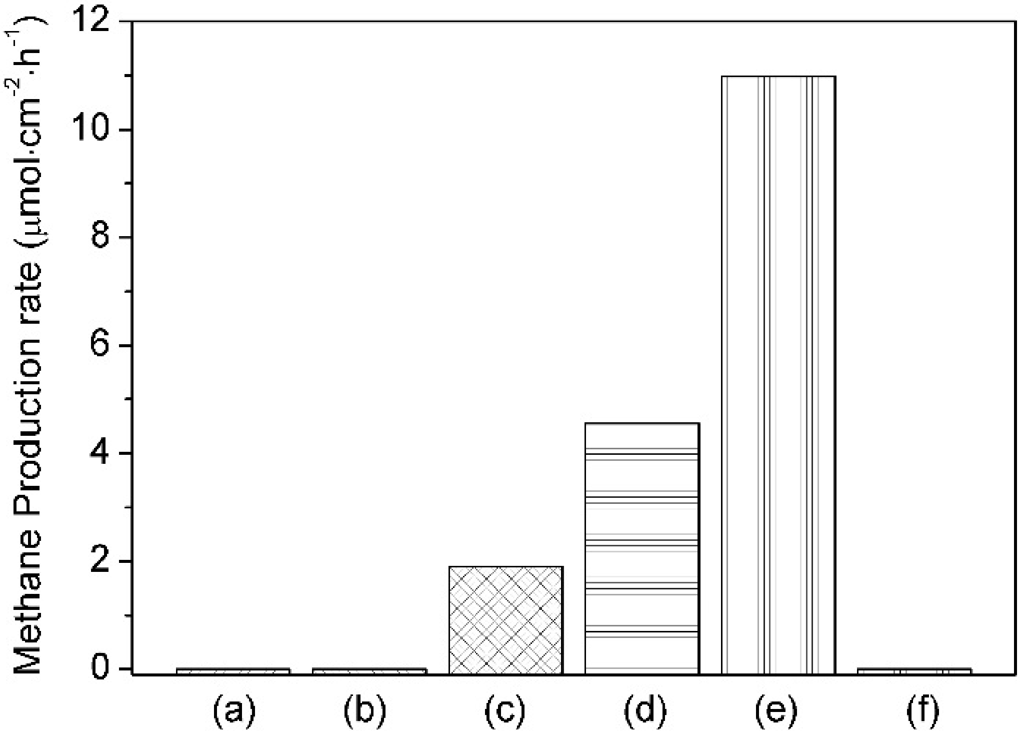

Figure 13. Rates of methane production (μmol·cm^{-2}·h^{-1}) under solar irradiation CO_2/H_2O(g) for (a) unannealed CuS dendrites, (b) annealed CuS dendrites (400 °C, 1 hour), (c) TiO_2 synthesized that Ti foil anodized at 3V for 1min and dried at 70 °C for 1 hour and annealed at 400 °C for 1 hour, (d) TiO_2 blocks-CuO nanorods (1 hour), (e) TiO_2 blocks-CuO nanorods (3 hours), and (f) TiO_2 blocks-CuO nanorods in CuO-TiO_2 in Ar/H_2O(g).

Also, control experiments show that there is no appreciable hydrocarbon production in the absence of either solar irradiation or photocatalysts, indicating that there are no significant thermal or photon effects, respectively. When tested in Ar/H_2O(g) instead of CO_2/H_2O(g), TiO_2 block-CuO nanorod tandem sample (f) shows no evidence of hydrocarbon production beyond the background noise of the measurement, suggesting that any organic impurities on the surface of the TiO_2 block-CuO nanorod tandem sample have negligible involvement in the CO_2 conversion reaction or on the reported methane production rates.

It is difficult to directly compare the methane production rate of the TiO_2 block-CuO nanorods tandem samples with rates reported for other photocatalysts because of the variance in experimental conditions, morphological features, surface areas, and co-catalysts. However, the catalytic performance of the TiO_2 block-CuO nanorod tandem sample is comparable to, and perhaps better than, other reported photocatalysts that convert CO_2 into methane using solar irradiation and without using noble metal co-catalysts.

5. CONCLUSIONS

The first study concluded that operation of a distinct CO_2 photoreactor have been demonstrated with simple mechanical design captivating the features of temperature and pressure control. The moderate yield of CH_4 as a main product advocates the reliability and efficient operation of newly installed experimental setup. Despite of significant progresses in the field of CO_2 photoreduction, it exhibits a challenging issue of diverse products ranging from CO to CH_4. One of the effective strategies to quick fix this dilemma is the development of hybrid photocatalysts leading to produce favorable hydrocarbon fuels.

The second study concluded that a novel strategy for synthesizing TiO_2 block - CuO nanorod tandem sample have been described, a new hybrid material that photocatalytically converts CO_2 into methane under solar irradiation. The synthetic strategy uses uniform CuO dendrites as both a TiO_2 precursor holder and compositional template for subsequent coating of TiO_2 precursor, oxidation of the TiO_2 block - CuO dendrites to form TiO_2 blocks decorated CuO nanorods tandem structures. Given this synthetic strategy and the design parameters that can be systematically varied, it should be possible to further improve the catalytic performance and to better understand nanostructure–property correlations in these and related materials.

References

[1] Jina Choi, Tae Sun Chang, and Beom-Sik Kim “Recent Development of Carbon Dioxide Conversion Technology.” *Clean Technology*, 18(3), 2012, pp. 229-249.

[2] Somnath C. Roy, Oomman K. Varghese., Maggie Paulose, and Craig A. Grimes “Toward Solar Fuels: Photocatalytic Conversion of Carbon Dioxide to Hydrocarbons.” *ACS nano*, 4, 2010, pp. 1259-1278.

[3] Zhen-Zhen Yang, Liang-Nian He, Jiao Gao, An-Hua Liu, and Bing Yu “Carbon dioxide utilization with C–N bond formation: carbon dioxide capture and subsequent conversion.” *Energy & Environmental Science*, 5, 2012, pp. 6602-6639.

[4] Kay Damen, Martijn van Troost, Andre´ Faaij, and Wim Turkenburg, “A comparison of electricity and hydrogen production systems with CO_2 capture and storage. Part A: Review and selection of promising conversion and capture technologies.” *Progress in Energy and Combustion Science*, 32, 2006, pp. 215-246.

[5] Tooru Inoue, Akira Fujishima, Satoshi Konishi, and Kenichi Honda, “Photoelectrocatalytic reduction of carbon dioxide in aqueous suspensions of semiconductor powder.” *Nature*, 277, 1979, pp. 637-638.

[6] Phong D. Tran, Lydia H. Wong, James Barber, and Joachim S. C. Loo “Recent advances in hybrid photocatalysts for solar fuel production.” *Energy & Environmental Science*, 5, 2012, pp. 5902-5918.

[7] Amarajothi Dhakshinamoorthy, Sergio Navalon, Avelino Corma, and Hermenegildo Garcia *Energy & Environmental Science*, 5, 2012, pp. 9217-9233.

[8] Albertus D Handoko, Kimfung Li, and Junwang Tang “Recent progress in artificial photosynthesis: CO_2 photoreduction to valuable chemicals in a heterogeneous system.” *Current Opinion in Chemical Engineering*, 2, 2013, pp. 200-206.

[9] Z. Jiang, T. Xiao, V. L. Kuznetsov, and P. P. Edwards “Turning carbon dioxide into fuel.” *Philosophical Transaction of the Royal Society A*, 368, 2010, pp. 3343-3364.

[10] Su-Il In, Dimitri D., Vaughn II., and Raymond E. Schaak “Hybrid CuO-$TiO_{2-x}N_x$ Hollow Nanocubes for Photocatalytic Conversion of CO_2 into Methane under Solar Irradiation.” *Angewandte Chemistry International Edition*, 51, 2012, pp. 3915-3918.

[11] Guohua Liu, Nils Hoivik, Kaiying Wangn, and Henrik Jakobsen “Engineering TiO_2 nanomaterials for CO_2 conversion/solar fuels.” *Solar Energy Materials & Solar Cells*, 105, 2012, pp. 53-68.

[12] Kohsuke Mori, Hiromi Yamashita, and Masakazu Anpo “Photocatalytic reduction of CO_2 with H_2O on various titanium oxide photocatalysts.” *RSC Advances*, 2, 2012, pp. 3165-3172.

[13] Suil In, Alexander Orlov, Regina Berg, Felipe Garcı´a, Sergio Pedrosa-Jimenez, Dominic S. Wright, Richard M. Lambert, and Mintcho S. Tikhov “Effective Visible Light-Activated B-Doped and B,N-Codoped TiO_2 Photocatalysts.” *Journal of the American Chemical Society*, 129, 2007, pp. 13790-13791.

[14] Christopher Vernona, Erica Thompsonb, and Sarah Cornella “Carbon dioxide emission scenarios: limitations of the fossil fuel resource.” *Procedia Environmental Sciences*, 6, 2011, pp. 206-215.

[15] Roddie R. Judkins, and William Fulkerson “The Dilemma of Fossil Fuel Use and Global Climate Change.” *Energy & Fuels*, 7, 1993, pp. 14-22.

[16] Richard S. Lindzen “Some remarks on global warming.” *Energy & Environmental Science*,

24(4), 1990, pp. 424-425.
[17] Fernando Fresno, Raquel Portela, Silvia Su´arez, and Juan M. Coronado "Photocatalytic materials: recent achievements and near future trends." *Journal of Materials Chemistry A*, 2, 2014, pp. 2863-2884.
[18] Evgenii V. Kondratenko, Guido Mul, Jonas Baltrusaitis, Gast´on O. Larraz´abal, and Javier P´erez-Ram´ırez "Status and perspectives of CO_2 conversion into fuels and chemicals by catalytic, photocatalytic and electrocatalytic processes." *Energy & Environmental Science*, 6, 2013, pp. 3112-3135.
[19] Venkata Pradeep Indrakanti, James D. Kubicki, and Harold H. Schobert "Photoinduced activation of CO_2 on Ti-based heterogeneous catalysts: Current state, chemical physics-based insights and outlook." *Energy & Environmental Science*, 2, 2009, pp. 745-758.
[20] Jin Mao, Kan Li, and Tianyou Peng "Recent advances in the photocatalytic CO_2 reduction over semiconductors." *Catalysis Science & Technology*, 3, 2013, pp. 2481-2498.
[21] Marı´a D. Hernandez-Alonso, Fernando Fresno, Silvia Suareza, and Juan M. Coronado "Development of alternative photocatalysts to TiO_2: Challenges and opportunities." *Energy & Environmental Science*, 2, 2009, pp. 1231-1257.
[22] Wonyong Choi, Andreas Termin, and Michael R. Hoffmann "The Role of Metal Ion Dopants in Quantum-Sized TiO_2: Correlation between Photoreactivity and Charge Carrier Recombination Dynamics." *The Journal of Physical Chemistry*, 98, 1994, pp. 13669-13679.
[23] Yasuo Izumi "Recent advances in the photocatalytic conversion of carbon dioxide to fuels with water and/or hydrogen using solar energy and beyond." *Coordination Chemistry Reviews*, 257, 2013, pp. 171-186.
[24] Xiukai Li, Zongjin Zhuanga, Wei Li, and Huiqi Pan "Photocatalytic reduction of CO_2 over noble metal-loaded and nitrogen-doped mesoporous TiO_2." *Applied Catalysis A: General*, 429– 430, 2012, pp. 31-38.
[25] Shunji Xie, Yu Wang, Qinghong Zhang, Wenqing Fan, Weiping Deng, and Ye Wang "Photocatalytic reduction of CO_2 with H_2O: significant enhancement of the activity of Pt-TiO_2 in CH_4 formation by addition of MgO." *Chemical Communication*, 49, 2013, pp. 2451-2453.
[26] Cunyu Zhao, Andy Krall, Huilei Zhao, Qianyi Zhang, and Ying Li "Ultrasonic spray pyrolysis synthesis of Ag/TiO_2 nanocomposite photocatalysts for simultaneous H_2 production and CO_2 reduction." *International Journal of Hydrogen Energy*, 37, 2012, pp. 9967-9976.
[27] S. Sonia, Naidu Dhanpal Jayram, P. Suresh Kumar, D. Mangalaraj, N. Ponpandian, and C. Viswanathan "Effect of NaOH concentration on structural, surface and antibacterial activity of CuO nanorods synthesized by direct sonochemical method." *Superlattices and Microstructures*, 66, 2014, pp. 1-9.
[28] J. Bandara, C. P. K. Udawatta, and C. S. K. Rajapaksea "Highly stable CuO incorporated TiO_2 catalyst for photocatalytic hydrogen production from H_2O." *Photochemical & Photobiological Sciences*, 4, 2005, pp. 857-861.
[29] Shiping Xu, Alan Jianhong Du, Jincheng Liu, Jiawei Ng, and Darren Delai Sun "Highly efficient CuO incorporated TiO_2 nanotube photocatalyst for hydrogen production from water." *International Journal of Hydrogen Energy*, 36, 2011, pp. 6560-6568.
[30] Shiping Xu, and Darren Delai Sun "Significant improvement of photocatalytic hydrogen generation rate over TiO_2 with deposited CuO." *International Journal of Hydrogen Energy*, 34, 2009, pp. 6096-6104.
[31] Yongquan Qu, and Xiangfeng Duan "One-dimensional homogeneous and heterogeneous nanowires for solar energyconversion." *Journal of Materials Chemistry*, 22, 2012, pp. 16171-16181.
[32] Bo Weng, Siqi Liu, Zi-Rong Tang, and Yi-Jun Xu "One-dimensional nanostructure based materials for versatile photocatalytic applications." *RSC Advances*, 4, 2014, pp. 12685-12700.

[33] Gopal K. Mor, Oomman K. Varghese, Maggie Paulose, Karthik Shankar, and Craig A. Grimes "A review on highly ordered, vertically oriented TiO_2 nanotube arrays: Fabrication, material properties, and solar energy applications." *Solar Energy Materials & Solar Cells*, 90, 2006, pp. 2011-2075.

[34] Jia Grace Lu, Paichun Chang, and Zhiyong Fan "Quasi-one-dimensional metal oxide materials—Synthesis, properties and applications." *Materials Science and Engineering R*, 52, 2006, pp. 49-91.

[35] Yu Li, Xiao-Yu Yang, Yi Feng, Zhong-Yong Yuan, and Bao-Lian Su "One-Dimensional Metal Oxide Nanotubes, Nanowires, Nanoribbons, and Nanorods: Synthesis, Characterizations, Properties and Applications." *Critical Reviews in Solid State and Materials Sciences*, 37, 2012, pp. 1-74.

[36] Valentina Krylova, andMindaugas Andruleviˇcius "Optical, XPS and XRD Studies of Semiconducting Copper Sulfide Layers on a Polyamide Film." *International Journal of Photoenergy*, 2009, 2009, pp. 1-8.

[37] Ang Li, Huaihe Song, Jisheng Zhou, Xiaohong Chen, and Siyuan Liu "CuO nanowire growth on Cu_2O by in situ thermal oxidation in air." *CrystEngComm*, 15, 2013, pp. 8559-8564.

[38] Jiangtao Hu, Teri Wang Odom, and Charles M. Lieber "Chemistry and Physics in One Dimension: Synthesis and Properties of Nanowires and Nanotubes." *Accounts of Chemical Research*, 32, 1999, pp. 435-445.

[39] Ai-Ping Jia, Shi-Yu Jiang, Ji-Qing Lu, and Meng-Fei Luo "Study of Catalytic Activity at the CuO-CeO_2 Interface for CO Oxidation." *The Journal of Physical Chemistry*, 114, 2010, pp. 21605-21610.

[40] Qiang Huang, Feng Kang, Hao Liu, Quan Li, and Xudong Xiao "Highly aligned Cu_2O/CuO/TiO_2 core/shell nanowire arrays as photocathodes for water photoelectrolysis." *Journal of Materials Chemistry A*, 1, 2013, pp. 2418-2425.

[41] Sreenivasan Koliyat Parayil, Harrison S. Kibombo, Chia-Ming Wu, Rui Peng, Jonas Baltrusaitis, and Ranjit T. Koodali "Enhanced photocatalytic water splitting activity of carbon-modified TiO_2 composite materials synthesized by a green synthetic approach." *International Journal of Hydrogen Energy*, 37, 2012, pp. 8257-8267.

[42] Ang Li, Huaihe Song, Wenbo Wan, Jisheng Zhou, and Xiaohong Chen "Copper oxide nanowire arrays synthesized by in-situ thermal oxidation as an anode material for lithium-ion batteries." *Electrochimica Acta*, 132, 2014, pp. 42-48.

[43] Sujun Yuan, Jiuke Mu, Ruiyi Mao, Yaogang Li, Qinghong Zhang, and Hongzhi Wang "All-Nanoparticle Self-assembly ZnO/TiO_2 Heterojunction Thin Films with Remarkably Enhanced Photoelectrochemical Activity." *ACS Applied Materials & Interfaces*, 6, 2014, pp. 5719-5725.

요 약 문

인공광합성: 광화학적 이산화탄소의 탄화수소 연료로의 전환

최근 환경 문제로 대기 중에 급격히 증가하는 이산화탄소 농도가 대두되고 있다. 대기 중의 이산화탄소를 유용한 자원으로 전환시켜 감소시키는 방법으로 열화학적, 광화학적 방법을 이용하는데, 그 중 광화학적전환은 환경 친화적이고 이산화탄소의 광환원으로 메탄올 포름알데히드, 메탄 가스와 같은 유용한 연료로 전환할 수 있어 주목 받고 있다. 광촉매의 표면에서 발생하는 이산화탄소의 탄화수소로의 광화학적 전환은 광촉매 영역의 획기적인 발견 중 하나이다. 현재 이산화탄소 전환효율을 증가시키기 위해 다양하게 접근하여 연구를 진행하고 있다. 이산화탄소 광전환을 위한 반응기는 실험장치에서 중요한 역할을 한다. 그래서 첫 번째 연구에서는 이산화탄소를 유용한 자원으로 전환시키기 위한 새롭게 설계된 광반응기를 제작했다. 광반응기는 특별히 간단히 온도를 측정하고 압력을 조절할 수 있도록 제작되었다. 제작된 광반응기를 시험해 보기 위해 Degussa P25 이산화티탄을 광촉매로 하여 365nm 에서 최대강도를 갖는 자외선 램프를 이용해 이산화탄소를 1007 $\mu mol \cdot g^{-1} \cdot h^{-1}$ (16.11 $ppm \cdot g^{-1} \cdot h^{-1}$)의 메탄으로 성공적으로 전환했다. 두번째 연구에서는 하이브리드 나노구조 $CuO-TiO_2$ 를 합성하여 이산화탄소 광전환을 실험했다. 전기화학적 양극산화를 통해 구리 호일에 황화 구리 구조체를 합성하고 티탄 전구체인 titanium isopropoxide 로 표면을 덮었다. 그 뒤 400 도에서 열처리를 하여 나노구조 $CuO-TiO_2$ 를 제작했다. 합성된 광촉매를 첫 번째 연구에서 제작한 광반응기 시스템을 이용해 태양광 모의 장치 아래에서 이산화탄소를 메탄으로 전환하는 실험에 성공했다.

핵심어: 광촉매, 이산화탄소 전환, 인공광합성, 광반응기, 텐덤형 $CuO-TiO_2$ 나노구조